Noninvasive prediction of tumor responses to gemcitabine using positron emission tomography

Rachel E. Laing[a,b], Martin A. Walter[c], Dean O. Campbell[a,b], Harvey R. Herschman[a,b], Nagichettiar Satyamurthy[a], Michael E. Phelps[a,b], Johannes Czernin[a,c], Owen N. Witte[a,d,1], and Caius G. Radu[a,b,1]

[a]Department of Molecular and Medical Pharmacology, [b]Crump Institute for Molecular Imaging, [c]Ahmanson Biological Imaging Division, and [d]Howard Hughes Medical Institute, and Department of Microbiology, Immunology, and Molecular Genetics, David Geffen School of Medicine, University of California, Los Angeles, CA 90095

Contributed by Owen N. Witte, December 18, 2008 (sent for review December 2, 2008)

Gemcitabine (2′,2′-difluorodeoxycytidine, dFdC) and cytosine arabinoside (cytarabine, ara-C) represent a class of nucleoside analogs used in cancer chemotherapy. Administered as prodrugs, dFdC and ara-C are transported across cell membranes and are converted to cytotoxic derivatives through consecutive phosphorylation steps catalyzed by endogenous nucleoside kinases. Deoxycytidine kinase (DCK) controls the rate-limiting step in the activation cascade of dFdC and ara-C. DCK activity varies significantly among individuals and across different tumor types and is a critical determinant of tumor responses to these prodrugs. Current assays to measure DCK expression and activity require biopsy samples and are prone to sampling errors. Noninvasive methods that can detect DCK activity in tumor lesions throughout the body could circumvent these limitations. Here, we demonstrate an approach to detecting DCK activity in vivo by using positron emission tomography (PET) and ^{18}F-labeled 1-(2′-deoxy-2′-fluoroarabinofuranosyl) cytosine] ([^{18}F]FAC), a PET probe recently developed by our group. We show that [^{18}F]FAC is a DCK substrate with an affinity similar to that of dFdC. In vitro, accumulation of [^{18}F]FAC in murine and human leukemia cell lines is critically dependent on DCK activity and correlates with dFdC sensitivity. In mice, [^{18}F]FAC accumulates selectively in DCK-positive vs. DCK-negative tumors, and [^{18}F]FAC microPET scans can predict responses to dFdC. We suggest that [^{18}F]FAC PET might be useful for guiding treatment decisions in certain cancers by enabling individualized chemotherapy.

[^{18}F]FAC | individualized chemotherapy | molecular imaging | deoxycytidine kinase

Development of new diagnostic, patient stratification, and treatment-monitoring approaches will accelerate the implementation of personalized therapy in cancer. Positron emission tomography (PET) using [^{18}F]fluorodeoxyglucose ([^{18}F]FDG) measures drug-induced changes in tumor glucose metabolism that correlate with clinical end points of treatment efficacy (reviewed in ref. 1). Such "metabolic responses" are detected earlier than changes in tumor volumes assessed by computed tomography (CT) (2–5). [^{18}F]FDG PET has been validated as an indicator of therapeutic responses in gastrointestinal stromal tumors (4, 5), high-grade soft tissue sarcomas (3), metastatic breast cancer (6), lung cancer (7), and adenocarcinoma of the esophagogastric junction (8).

In addition to treatment monitoring, PET may also prove useful in guiding therapeutic decisions before treatment initiation. Measurements of estrogen receptor expression by using [^{18}F]fluoroestradiol PET could be useful for stratifying breast cancer patients for estrogen-based therapy (9, 10). PET using [4-^{18}F]fluorobenzaldehyde-conjugated aminooxy-protein scaffolds has been used in small animal models to detect tumoral Her2 expression (11). Similar approaches could guide the selection of chemotherapy regimes. However, PET probes that can measure the activity of proteins or biochemical pathways targeted by common chemotherapy drugs are lacking. If available, such probes could enable pretherapeutic stratification of patients and reduce the frequency of ineffective chemotherapy.

To develop PET probes and assays that are predictive of responses to chemotherapy, we focused on a class of pyrimidine and purine nucleoside prodrugs represented by gemcitabine [2′,2′-difluorodeoxycytidine (dFdC, Gemzar)] and cytosine arabinoside (ara-C) (Fig. 1*A*). These and related compounds fludarabine, cladribine (Leustatin), and clofarabine (Evoltra /Clolar) are used in solid and hematologic malignancies (reviewed in ref. 12). A shared feature of these prodrugs concerns their critical requirement for deoxycytidine kinase (DCK, EC 2.7.1.74) activity to initiate their conversion from inactive prodrugs to cytotoxic derivatives. DCK phosphorylates dFdC, ara-C, and related prodrugs and thereby traps them intracellularly (Fig. 1*A*).

The efficacy of the dFdC and ara-C class of prodrugs is limited by several resistance mechanisms (reviewed in ref. 13), with low DCK activity playing a major role (14–16). Single-nucleotide polymorphisms in the regulatory region (rSNPs) of DCK correlate with responses to ara-C in acute myeloid leukemia (AML) (17). Other rSNPs correlate with low DCK expression and lower blast ara-C-5′-triphosphate levels in AML patients receiving ara-C as continuous infusion (18). Treatment-induced resistance to dFdC has been documented in cell lines and animal models (reviewed in ref. 19). dFdC-treated patients with tumors expressing low levels of DCK have shorter survival rates compared with those with tumors expressing high levels of this enzyme (20, 21). Previous studies show a good correlation among measurements of tumor DCK mRNA (22), protein (23), and enzymatic activity (15), and responses to dFdC and ara-C. However, the accuracy of such invasive methods is limited by sampling errors caused by disease heterogeneity, both within a large tumor and between different tumor lesions or metastases. A noninvasive method to visualize DCK activity throughout the body could circumvent this limitation.

Herein we describe a PET imaging approach for noninvasive detection of DCK activity and prediction of tumor responses to dFdC. We recently developed ^{18}F-labeled 1-(2′-deoxy-2′-fluoroarabinofuranosyl) cytosine ([^{18}F]FAC; Fig. 1*A*), a PET probe that is sensitive to changes in lymphoid mass and immune

Author contributions: R.E.L., M.A.W., D.O.C., H.R.H., M.E.P., J.C., O.N.W., and C.G.R. designed research; R.E.L. and D.O.C. performed research; N.S. contributed new reagents/analytic tools; R.E.L., M.A.W., D.O.C., and C.G.R. analyzed data; and R.E.L., H.R.H., O.N.W., and C.G.R. wrote the article.

Conflict of interest statement: C.G.R., N.S., J.C., and O.N.W. are among the inventors of the national and PCT patent applications for the FAC technology referred to in the article. That patent application was filed on September 19, 2008. A group of UCLA faculty members including C.G.R., N.S., J.C., M.E.P., and O.N.W. are involved in a startup company that is negotiating for the license to this intellectual property.

Freely available online through the PNAS open access option.

[1]To whom correspondence may be addressed. E-mail: owenw@microbio.ucla.edu or cradu@mednet.ucla.edu.

This article contains supporting information online at www.pnas.org/cgi/content/full/0812890106/DCSupplemental.

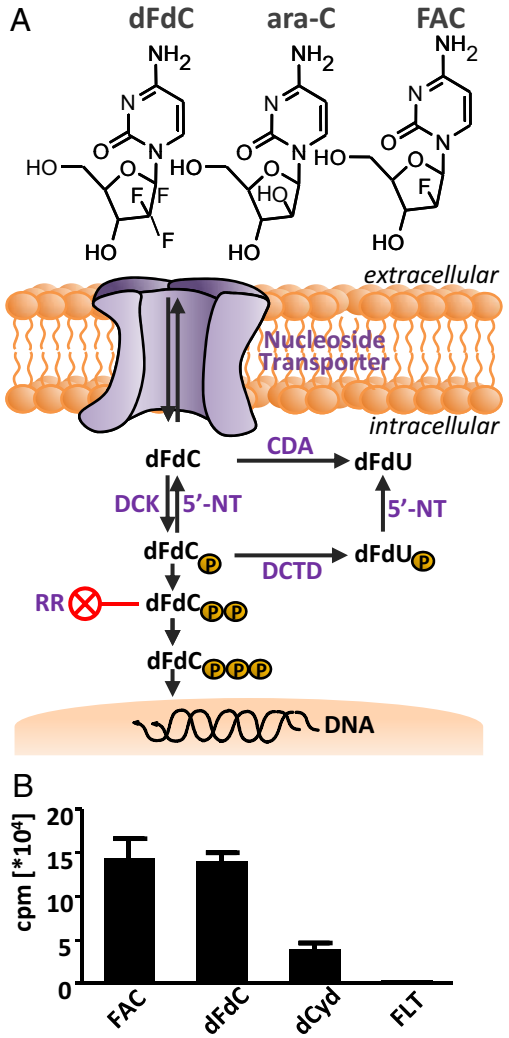

Fig. 1. The DCK-dependent nucleoside salvage pathway and evaluation of FAC as a substrate for DCK. (*A*) Chemical structures of dFdC, ara-C, and FAC, and schematic of dFdC uptake and activation. 5′-NT, 5′-nucleotidase; DCTD, dCMP deaminase; RR, ribonucleotide reductase. (*B*) In vitro kinase assay with purified recombinant DCK enzyme showing that FAC is a specific substrate.

activation in animal models (24). [^{18}F]FAC was identified by differential screening of nucleoside analogs for preferential retention in activated vs. naïve T lymphocytes (24). We showed that ectopic overexpression of DCK in NIH 3T3 fibroblasts increased the uptake of FAC and dFdC, suggesting that these related nucleoside analogs might be metabolized in a similar manner (24). This led us to hypothesize that [^{18}F]FAC microPET may allow noninvasive detection of DCK activity in vivo and that [^{18}F]FAC retention in tumors measured by PET could correlate with dFdC sensitivity.

We report that (*i*) similar to dFdC, FAC is a high-affinity substrate for DCK; (*ii*) in vitro, retention of FAC in human and mouse leukemic cell lines correlates with DCK expression and activity as well as with responses to dFdC; and (*iii*) pretreatment [^{18}F]FAC microPET/CT scans distinguish DCK-positive and -negative tumors in vivo and predict responses to dFdC. These results suggest that [^{18}F]FAC PET may represent a step toward individualized chemotherapy by enabling biochemical stratification of tumor lesions to provide noninvasive imaging biomarkers that are predictive of sensitivity to dFdC, ara-C, and related prodrugs.

Table 1. Enzyme kinetic data for DCK

Kinetic parameter	FAC	dFdC	dCyd
V_{max}, nmol/min per mg	218.9 ± 0.3	162.0 ± 1.0	247.2 ± 12.4
K_m, μM	0.34 ± 0.13	0.98 ± 0.50	1.05 ± 0.31
K_{cat}, $\times 10^5$ s^{-1}	2.4	1.8	2.7

Results

FAC, a Recently Developed PET Probe, Is a High-Affinity Substrate for DCK. To investigate whether FAC (Fig. 1*A*) is a substrate for DCK, we performed kinase assays using purified recombinant enzyme. dFdC and the endogenous DCK substrate 2′-deoxycytidine (dCyd) were used as positive controls. Fluoro-L-thymidine (FLT), a thymidine kinase 1-specific substrate, was used as a negative control. DCK phosphorylated FAC and dFdC to a similar degree, whereas FLT was not phosphorylated (Fig. 1*B*). The kinetic parameters of recombinant DCK for dCyd [Table 1 and supporting information (SI) Fig. S1] were similar to published data (25). FAC displayed a lower K_m value than dCyd (0.34 μM vs. 1.05 μM) with a similar V_{max} value (218.9 nmol/min per mg vs. 247.2 nmol/min per mg).

FAC Retention in Leukemic Cells Is Critically Dependent on DCK Activity and Correlates with Sensitivity to dFdC. To investigate the relationship between FAC retention and DCK activity, we used isogenic cell lines expressing various levels of DCK. The L1210 model consists of the DCK-positive wild-type (L1210 wt) line and the DCK-deficient subline L1210-10K (14). We used retroviral transduction to restore DCK expression in the L1210-10K cells (L1210-10K+DCK; Fig. 2*A*). L1210 wt cells were sensitive to dFdC, whereas the DCK-deficient line was >15,000-fold resistant. Adding back DCK to the L1210-10K line completely restored dFdC sensitivity (Fig. 2*B* and Table S1). L1210 wt cells phosphorylated FAC, whereas L1210-10K cells did not ($P < 0.001$). DCK-deficient cell lines reconstituted with DCK showed enhanced phosphorylation of FAC (224% relative to L1210 wt cells, $P < 0.001$), consistent with the increased DCK expression (Fig. 2 *A* and *C*). The pattern of dFdC phosphorylation in these cell lines was similar to that of FAC (Fig. 2*C*). To detect phosphorylated FAC metabolites, kinase reaction products were analyzed by HPLC (Fig. S2). L1210 wt samples yielded two peaks consisting of FAC and FAC-monophosphate (FAC-MP, with a FAC to FAC-MP ratio of 1.5), whereas L1210-10K samples yielded a single peak corresponding to FAC.

Radioactive tracer uptake assays using [^{3}H]FAC and [^{3}H]-dFdC were performed for each cell line. The DCK-positive L1210 wt cell line displayed substantial uptake of both FAC and dFdC, whereas L1210-10K cells did not take up FAC or dFdC (Fig. 2*D*; $P < 0.001$). Reintroduction of DCK in the L1210-10K cells restored the uptake of both FAC and dFdC above wild-type levels (Fig. 2*D*; 230% and 316% over wild-type cells for FAC and dFdC, respectively, $P < 0.001$). FLT and 2-deoxyglucose (2-DG), which are not substrates for DCK, showed similar uptake in all three cell lines (Fig. 2*E*).

To determine whether the results in the murine L1210 system could be extended to human cell lines, we used the lymphoma line CCRF-CEM (CEM wt), and its DCK-deficient variant, CEM-R (26). CEM wt cells were sensitive to dFdC (IC_{50} 0.049 μM), whereas CEM-R cells were highly resistant (IC_{50} 8.0 mM). Adding back DCK in CEM-R cells (CEM-R+DCK) partially restored sensitivity to dFdC (IC_{50} 2.05 μM) (Table S1). CEM wt cells phosphorylated FAC and dFdC, whereas CEM-R cells did not ($P < 0.001$). CEM-R+DCK cells phosphorylated FAC and dFdC to at least 50% of wild-type levels ($P < 0.001$) (Fig. S3 *A* and *B*). Accordingly, the DCK-positive CEM wt cells showed higher FAC and dFdC uptake compared with the DCK-deficient

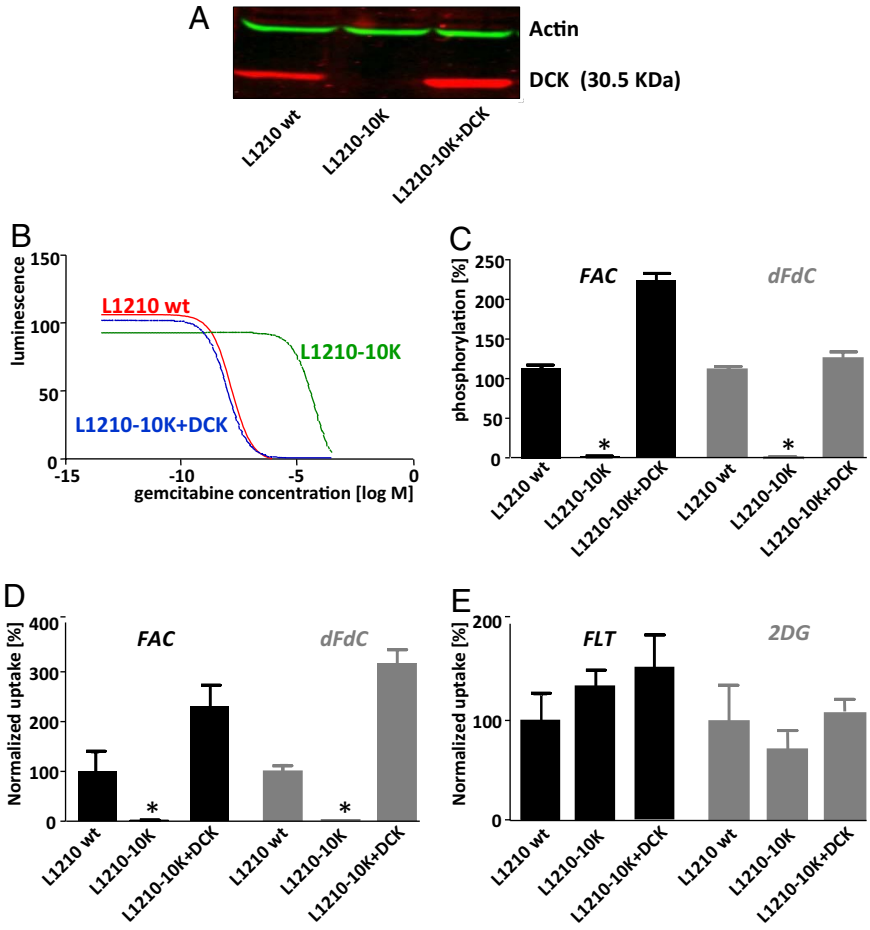

Fig. 2. FAC phosphorylation and retention require DCK expression. (*A*) Western blot of cell lines probed with anti-DCK and anti-actin antibodies. (*B*) IC_{50} dFdC curves of the L1210 cell line panel. DCK-expressing cells display greater sensitivity to dFdC than DCK-deficient cells. Data are fitted as log (inhibitor) vs. response. (*C*) In vitro kinase assay with the L1210 cell lines with 1 μCi of [^{18}F]FAC (*Left*) and [^{3}H]dFdC (*Right*) as a substrate (1 μg of protein per reaction). (*D* and *E*) In vitro uptake assays with 1 μCi of ^{3}H-labeled probes in the L1210 cell lines; 2-DG and FLT were negative controls.

CEM-R cells ($P < 0.001$). Adding back DCK to CEM-R cells did not rescue FAC ($P = 0.03$) and dFdC ($P = 0.03$) uptake to levels seen in the CEM wt cells, in accordance with the partial phosphorylation rescue (Fig. S3*C*). FLT uptake was also decreased in the CEM-R cells relative to CEM wt cells ($P = 0.003$), reflecting their slower growth kinetics seen in cell culture (data not shown).

Stratification of DCK-Positive and -Negative Tumors by Using [^{18}F]FAC MicroPET/CT and Noninvasive Prediction of Tumor Responses to dFdC. To determine whether [^{18}F]FAC microPET/CT can differentiate DCK-positive from DCK-negative tumors in vivo, L1210 wt and L1210-10K cells were implanted in SCID mice. We performed [^{18}F]FAC microPET/CT scans 6–7 days after tumor implantation. Mice were also scanned with [^{18}F]FDG to confirm the presence of metabolically active tumors. L1210 wt- and L1210-10K-derived tumors accumulated similar amounts of [^{18}F]FDG (L1210 wt, 13.4 ± 2.37% injected dose/g (ID/g); L1210-10K, 10.0 ± 4.05% ID/g) (Fig. 3 *A* and *C* and Fig. S4). In contrast, [^{18}F]FAC microPET/CT distinguished dFdC-sensitive (DCK-positive) tumors from dFdC-resistant (DCK-deficient) tumors (Fig. 3 *B* and *C* and Fig. S4). L1210 wt tumors showed significantly higher [^{18}F]FAC uptake (5.24 ± 1.13% ID/g) than L1210-10K tumors (0.242 ± 0.207% ID/g; $P < 0.001$; $n = 4$ mice per group; similar results were obtained in four independent experiments).

To determine the predictive value of [^{18}F]FAC microPET/CT, we established a dFdC treatment model in which L1210 wt and L1210-10K tumor-bearing mice were scanned before treatment initiation (Fig. 3*D*). Mice were then treated with dFdC (360 mg/kg), and tumor responses were assessed by caliper measurements and postmortem histological analysis. [^{18}F]FAC-positive L1210 wt tumors responded to dFdC and showed a significant decrease in volume compared with both untreated controls and dFdC-treated [^{18}F]FAC-negative L1210-10K tumors ($P < 0.001$), which increased in volume (Fig. 3*D*). Histological analysis showed that L1210 wt tumors from dFdC-treated mice displayed a mitotic index of 0, whereas tumors from control and L1210-10K tumor bearing mice displayed mitotic indexes with an average of 9 (data not shown).

Discussion

Noninvasive Imaging Predicts Tumor Responses to dFdC. In this article we demonstrate that [^{18}F]FAC microPET/CT detects a rate-limiting step in dFdC activation dependent on DCK activity. We show that [^{18}F]FAC is a high-affinity substrate for DCK and that, similar to dFdC, [^{18}F]FAC uptake and phosphorylation require DCK activity. Furthermore, the tumor uptake of [^{18}F]FAC measured by microPET/CT is predictive of dFdC efficacy in a murine leukemia model.

Potential Clinical Applications of [^{18}F]FAC PET. Molecular stratification of tumor lesions to guide therapeutic decisions is a major objective in oncology. Diagnostic tools that predict a patient's response to chemotherapy could reduce the use of noneffective

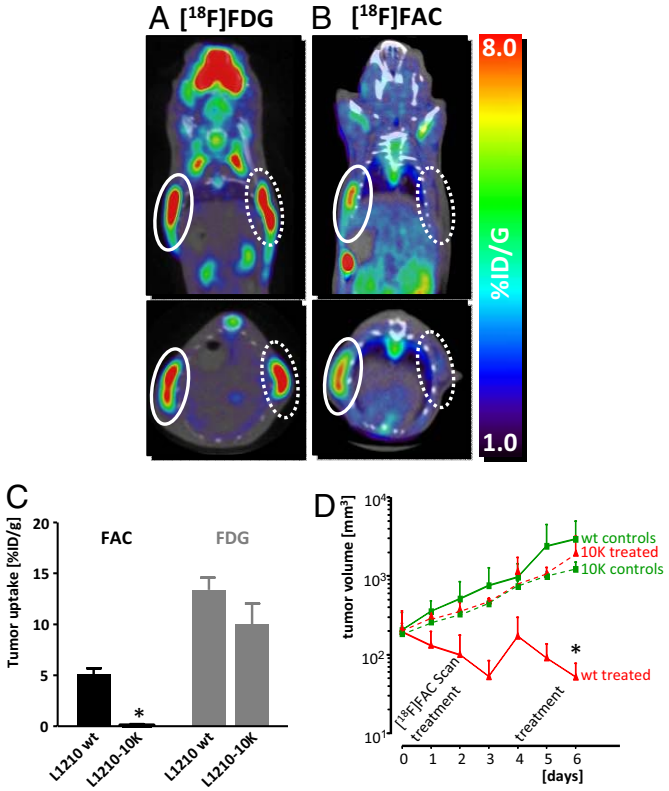

Fig. 3. [18F]FAC microPET/CT distinguishes DCK-positive and -negative tumors in vivo and predicts responses to dFdC. (*A*) [18F]FDG microPET/CT scans of L1210 wt and L1210-10K tumors in SCID mice. Mice were imaged 1 h after i.p. injection of probe. Solid white circles denote L1210 wt tumors, dotted white circles denote L1210-10K tumors. (*B*) [18F]FAC microPET/CT scans of the same mice, imaged 1 day after the [18F]FDG microPET/CT scans. (*C*) Quantification of tracer uptake in tumors was performed by drawing regions of interest (2 mm^3) at the tumor sites with Amide software. Data presented are from one experiment ($n = 4$ mice per group) that was repeated four times with reproducible results. (*D*) [18F]FAC microPET/CT can predict response to dFdC. SCID mice bearing either L1210 wt or L1210-10K tumors were paired for equal tumor size and randomized for treatment, receiving 360 mg/kg dFdC (on days 0 and 4) or no treatment ($n = 3$ per group). Caliper measurements were performed daily. Data are presented as tumor volumes over time (mm^3).

drugs and enable physicians to explore additional therapeutic options rapidly. dFdC is used in several hematopoietic malignancies and solid tumors. However, response rates are low and rarely exceed 20% (27, 28). Reported DCK enzymatic activity in tumors ranges from 5 to 18 pmol/h per mg of protein, and previous studies have found these values to correlate with sensitivity to dFdC (15, 29). The DCK activity in L1210 wt leukemia cells was 0.4 nmol/h per mg, well within the range observed in other tumors. Although our data indicate that [18F]FAC microPET can distinguish DCK-positive from DCK-negative cell lines and tumors, future studies are needed to determine whether this approach can also detect more subtle variations in DCK levels or other facets of tumor nucleoside metabolism. To detect the threshold of enzyme required to be predictive of dFdC response, tetracycline-regulated DCK expression in cell culture systems is being exploited. We are also generating conditional DCK-knockout mice to provide a model in which to study the effects of DCK inactivation and haploinsufficiency on the uptake of FAC. Finally, projected clinical studies will explore the correlation between DCK levels of tumor biopsies and the observed [18F]FAC signals.

In addition to dFdC, several other prodrugs also depend on DCK for their activation. Ara-C, cladribine, and fludarabine are used primarily in hematological malignancies. More recently, clofarabine and troxacitabine have been evaluated in clinical trials for various cancers (13). Thus, [18F]FAC PET may provide biomarkers for predicting responses to an entire class of related chemotherapeutic prodrugs. Patients who display low or undetectable tumoral uptake of [18F]FAC would be expected to show low response rates to these prodrugs and could be candidates for alternative chemotherapy regimes. Lack of [18F]FAC uptake may indicate that these tumors synthesize their DNA primarily via the de novo pathway rather than by using the DCK-dependent nucleoside salvage pathway. In turn, this may indicate that these patients could respond to therapies that interfere with the de novo pathway, including conventional drugs like hydroxyurea- and siRNA-based approaches that block the function of key enzymes in the de novo pathway such as ribonucleotide reductase (30–32).

Additional Mechanisms of dFdC Resistance and Potential Limitations of [18F]FAC PET. Other biochemical mechanisms in addition to DCK have been involved in dFdC resistance. dFdC is taken up via nucleoside transporters at the cell membrane (Fig. 1*A*). Down-regulation of the human equilibrative nucleoside transporter-1 (hENT-1; SLC29a1) was associated with lower response rates to dFdC (reviewed in ref. 13). Our previous data suggest that similar to dFdC, FAC is transported by SLC29a1 (24). Therefore, [18F]FAC PET may also enable detection of deficient dFdC transport. Experiments to validate the role of SLC29a1 in FAC uptake are ongoing in cell lines expressing mutant SLC29a1 and in isogenic cell lines with varying levels of transporter.

Quantitative tracer kinetic analyses (33) may be useful to determine the contribution of transport (SLC29A1-dependent) vs. phosphorylation (DCK-dependent) mechanisms to [18F]FAC tumor retention. Dynamic imaging studies of L1210 wt and L1210-10K tumors with [18F]FAC indicate that forward transport (*K*1) is similar between these tumors, whereas net retention (Ki) is significantly higher in the L1210 wt tumors vs. the L1210-10K tumors (Fig. S5). These findings suggest that kinetic analysis of [18F]FAC PET data could potentially be used to assess drug uptake. Such analyses could also be used to determine whether drugs shown to synergize with dFdC such as cisplatin (27) and pemetrexed (34) enhance dFdC uptake by tumor cells in vivo. In this context, treatment with dFdC induces a flare in FAC uptake in cell culture, similar to the flare reported for FLT (35). Our data indicate that L1210 wt cells display cell cycle arrest after 16 h of dFdC treatment and show increased FAC and FLT accumulation compared with the resistant L1210-10K cells (Fig. S6). These results warrant follow-up in vivo studies and suggest that posttherapy [18F]FAC PET imaging could be useful to monitor tumor responses to dFdC.

Elevated levels of cytidine deaminase (CDA) have been associated with dFdC and ara-C resistance (reviewed in ref. 13). CDA converts significant amounts of deoxycytidine-based prodrugs into inactive uracil metabolites (Fig. 1*A*). Elevated CDA expression has been associated with poor progression rate and survival in advanced pancreatic adenocarcinoma patients treated with dFdC (36). Similar to dFdC, FAC is also susceptible to deamination (D.O.C. and C.G.R., unpublished observation). Thus, [18F]FAC PET may provide a measurement of resistance caused by elevated CDA activity. In addition to CDA, overexpression of the ribonucleotide reductase subunit M1 (Fig. 1*A*) has also been implicated in dFdC resistance (37, 38). It is currently unknown whether [18F]FAC PET can detect this mechanism of resistance.

Another potential limitation of [18F]FAC PET concerns the possibility of false-positive results caused by the cross-reactivity of the probe with activated immune cells such as T lymphocytes (24). Further studies are warranted to determine whether the uptake of [18F]FAC by tumor lesions could reflect not only the

expression of DCK by cancer cells but also the presence of tumor-infiltrating immune cells. If correct, such false-positive results may reduce the positive predictive value of [^{18}F]FAC PET but should not affect its negative predictive value.

Concluding Remarks. The advent of personalized medicine has provided the impetus for the development of new imaging tools that can enable molecular stratification of tumor lesions and can be used to guide and monitor treatment. Several such approaches have been developed in recent years. Using phage display, Han *et al.* (39) have identified peptides that bind specifically to tumors that respond to a combination of antiangiogenic therapy and radiotherapy. Radiolabeled analogs of these peptides could be used for PET-based monitoring of early treatment responses (39). In addition to PET, other noninvasive imaging modalities such as MRI (40) and CT (41) could also prove useful. Finally, targeted radiotherapeutics, such as metaiodobenzylguanidine, have been used to identify patients with neuroblastoma or pheochromocytoma that will respond to radioiodine therapy (42).

Alone or in combination, PET, CT and MRI could represent the first step toward a "toolbox" of noninvasive imaging methods for patient stratification and individualized chemotherapy. In conjunction with gene expression profiling, high-throughput DNA sequencing, and proteomics, these imaging tools may have a significant impact in oncology.

Materials and Methods

Cell Lines and Drugs. The murine leukemic lines (L1210 wt and L1210-10K) (14) were a gift from Charles Dumontet (Université Claude Bernard Lyon I, Lyon, France). The human lymphoma line CCRF-CEM and its ara-C-resistant DCK-negative derivative line (CEM-R) (26) were provided by Margaret Black (Washington State University). All L1210 and CEM cell lines were cultured in RPMI medium 1640, supplemented with 5% FCS and 2 mM L-glutamine, in a 5% CO_2 37 °C incubator. The amphotrophic retrovirus packaging cell line Phoenix (American Type Culture Collection, SD 3443) was used for the production of murine stem cell virus-based retroviruses (43) containing enhanced GFP (eGFP) and human DCK. L1210-10K cells and CEM-R cells were transduced with retrovirus as described in ref. 24. The transduction efficiency was ≈50%, and cell sorting for eGFP expression using flow cytometry ensured a pure population of DCK-expressing cells. dFdC was obtained from the UCLA pharmacy, and stock solutions were prepared in 0.9% saline.

Antibodies and Western Blotting. Total cellular protein (30 μg) was subjected to SDS/PAGE on 12% wt/vol acrylamide gels (Bio-Rad). Protein was transferred to nitrocellulose membrane (88018; Pierce) that was blocked overnight at 4 °C in the LiCor blocking solution (927-40000; LiCor Biosciences). Membranes were probed with primary antibodies for 1 h at room temperature. The rabbit polyclonal antibody against DCK was provided by Françoise Bontemps (University Catholique de Louvain, Belgium) (44). The mouse anti-actin antibody (A4700; Sigma) was used as loading control. Membranes were washed with PBS-T (Tween 0.1% wt/vol), probed with an infrared dye-labeled secondary antibody (926-32210 and 926-32211; LiCor Biosciences) for 1 h, washed again with PBS-T, and then scanned by using the Odyssey infrared imaging system.

IC_{50} Assay. Cells were plated in 96-well plates (5×10^3 cells in 50 μL of medium) and allowed to settle for 1–3 h. Serial 5× drug dilutions of dFdC, starting at 400 μM, were prepared in RPMI medium 1640, and 50 μL of each dilution was added to cells, bringing the final volume to 100 μL per well. Cells were incubated for 72 h at 37 °C, 5% CO_2.The ATPlite assay (6016739; PerkinElmer) was used for IC_{50} measurements (45).

In Vitro Kinase and Uptake Assays. Recombinant DCK was purified from the *Escherichia coli* strain SØ441 (cdd- and urt-strain) that expresses human DCK in a pETHT vector (a gift from Margaret Black). Cellular protein was isolated from the L1210 and CEM cells lysed by consecutive freeze/thaw cycles. For in vitro kinase reactions, pure DCK or whole-cell lysates (0.2 μg/μL total protein) were incubated with 1 μCi of ^{3}H-labeled FAC, dFdC, dCyd, FLT (MT1858, MT1572, MT953, respectively; Moravek Biochemicals) or ^{18}F-labeled FAC. UTP was used as a phosphate donor (U6875; Sigma). Radioactivity was determined by using a Beckman scintillation counter (LS 6500). Kinetic analyses of the recombinant DCK were performed by using the Kinase-Glo Max luminescent kinase assay kit (V6071; Promega) (46). The protocol was adapted from a previous report (47). Briefly, kinase assays with purified recombinant DCK were performed in the presence of dCyd (0–300 μM), dFdC (0–300 μM), or FAC (0–228 μM) in 50 mM Tris (pH 7.6), 2 mM $MgCl_2$, and 3 mM ATP at 37 °C. After 30 min, reactions were stopped by heating to 95 °C for 5 min. The mixture was then cooled to room temperature and diluted 6-fold before the addition of the Kinase-Glo Max reagent. The luminescent output was measured by using the HT analyzer (PerkinElmer) plate reader. Radioactive tracer cell uptake assays were carried out as reported in ref. 24.

In Vivo Treatment Model and MicroPET/CT Imaging. All animal studies were carried out according to the guidelines of the Department of Laboratory Animal Medicine (DLAM) at UCLA. Male NOD SCID mice (CBySmn.CB17-Prkdcscid/J) were obtained from the Jackson Laboratories. Mice were injected s.c. with 2×10^6 cells, and tumors were allowed to develop for 7 days. Mice were then paired for matching tumor sizes and randomized in treatment vs. control groups. Treatment groups were treated with dFdC [360 mg/kg; i.p. (14)] on days 0 and on 4. Mice were scanned with [^{18}F]FDG (day −1) and [^{18}F]FAC (day 0) before treatment. Mice were killed after imaging on day 6, and tumors were removed for histology to determine the mitotic index. Imaging protocols are described in *SI Materials and Methods* and were carried out as described in ref. 24.

Statistical Analyses. Data are presented as means ± SEM. Multiple group comparisons were performed by using Student's *t* test. IC_{50} curves were calculated by using a nonlinear regression model [log (inhibitor) vs. response]. All *P* values are two-sided, and *P* values of <0.05 are considered to be statistically significant. Data were analyzed by using Statistica version 6.0 software for Windows (StatSoft) and SPSS release 14.0 (SAS Institute). Graphs were generated by using the GraphPad Prism 5 software.

ACKNOWLEDGMENTS. We thank D. Stout, W. Ladno, B. Chun, and J. Edwards for microPET/CT imaging and the cyclotron group for the production of PET probes; G. Toy, M. Riedinger, and J. Wengrod for technical assistance; C. J. Shu and J. Lee for generating HPLC data; I. J. Hildebrandt for animal and imaging expertise; H. Huang and K. P. Wong for dynamic imaging analysis; A. Tran and B. Anderson for help with manuscript preparation; and the Jonsson Comprehensive Cancer Center Flow Cytometry Facility at UCLA. We are grateful to Dr. Dumontet for the L1210 wt and L1210-10K cell lines, Dr. Black for providing the *E. coli* strain expressing the pETHT-human DCK plasmid, and Dr. Bontemps for providing the anti-DCK antibody. O.N.W. is an Investigator of the Howard Hughes Medical Institute. This work was supported by In Vivo Cellular and Molecular Imaging Centers Developmental Project Award NIH P50 CA86306 (to C.G.R., D.O.C., and R.E.L.), National Cancer Institute/National Institutes of Health Grants 5U54 CA119347 (to C.G.R.) and R24CA92865, U.S. Department of Energy Contract DE-FG02-06ER64249 (to M.E.P.), and the Dana Foundation (C.G.R.). C.G.R. received unrestricted support from Merck Research Laboratories.

1. Contag CH (2007) In vivo pathology: Seeing with molecular specificity and cellular resolution in the living body. *Annu Rev Pathol* 2:277–305.
2. Weber WA, Czernin J, Phelps ME, Herschman HR (2008) Technology insight: Novel imaging of molecular targets is an emerging area crucial to the development of targeted drugs. *Nat Clin Pract* 5:44–54.
3. Evilevitch V, *et al.* (2008) Reduction of glucose metabolic activity is more accurate than change in size at predicting histopathologic response to neoadjuvant therapy in high-grade soft-tissue sarcomas. *Clin Cancer Res* 14:715–720.
4. Gayed I, *et al.* (2004) The role of ^{18}F-FDG PET in staging and early prediction of response to therapy of recurrent gastrointestinal stromal tumors. *J Nucl Med* 45:17–21.
5. Goerres GW, *et al.* (2005) The value of PET, CT, and in-line PET/CT in patients with gastrointestinal stromal tumours: Long-term outcome of treatment with imatinib mesylate. *Eur J Nucl Med Mol Imaging* 32:153–162.
6. Dose Schwarz J, *et al.* (2005) Early prediction of response to chemotherapy in metastatic breast cancer using sequential ^{18}F-FDG PET. *J Nucl Med* 46:1144–1150.
7. Weber WA, *et al.* (2003) Positron emission tomography in non-small-cell lung cancer: Prediction of response to chemotherapy by quantitative assessment of glucose use. *J Clin Oncol* 21:2651–2657.
8. Lordick F, *et al.* (2007) PET to assess early metabolic response and to guide treatment of adenocarcinoma of the oesophagogastric junction: The MUNICON phase II trial. *Lancet Oncol* 8:797–805.
9. Peterson LM, *et al.* (2008) Quantitative imaging of estrogen receptor expression in breast cancer with PET and ^{18}F-fluoroestradiol. *J Nucl Med* 49:367–374.
10. Linden HM, *et al.* (2006) Quantitative fluoroestradiol positron emission tomography imaging predicts response to endocrine treatment in breast cancer. *J Clin Oncol* 24:2793–2799.
11. Cheng Z, *et al.* (2008) Small-animal PET imaging of human epidermal growth factor receptor type 2 expression with site-specific ^{18}F-labeled protein scaffold molecules. *J Nucl Med* 49:804–813.
12. Faderl S, *et al.* (2005) The role of clofarabine in hematologic and solid malignancies: Development of a next-generation nucleoside analog. *Cancer* 103:1985–1995.

13. Jordheim LP, Dumontet C (2007) Review of recent studies on resistance to cytotoxic deoxynucleoside analogues. *Biochim Biophys Acta* 1776:138–159.
14. Jordheim LP, *et al.* (2004) Characterization of a gemcitabine-resistant murine leukemic cell line: Reversion of in vitro resistance by a mononucleotide prodrug. *Clin Cancer Res* 10:5614–5621.
15. Kroep JR, *et al.* (2002) Pretreatment deoxycytidine kinase levels predict in vivo gemcitabine sensitivity. *Mol Cancer Ther* 1:371–376.
16. Galmarini CM, *et al.* (2004) Resistance to gemcitabine in a human follicular lymphoma cell line is due to partial deletion of the deoxycytidine kinase gene. *BMC Pharmacol* 4:8.
17. Shi JY, *et al.* (2004) Association between single nucleotide polymorphisms in deoxycytidine kinase and treatment response among acute myeloid leukaemia patients. *Pharmacogenetics* 14:759–768.
18. Lamba JK, *et al.* (2007) Pharmacogenetics of deoxycytidine kinase: Identification and characterization of novel genetic variants. *J Pharmacol Exp Ther* 323:935–945.
19. Bergman AM, Pinedo HM, Peters GJ (2002) Determinants of resistance to 2′,2′-difluorodeoxycytidine (gemcitabine). *Drug Resist Update* 5:19–33.
20. Sebastiani V, *et al.* (2006) Immunohistochemical and genetic evaluation of deoxycytidine kinase in pancreatic cancer: Relationship to molecular mechanisms of gemcitabine resistance and survival. *Clin Cancer Res* 12:2492–2497.
21. Ueno H, Kiyosawa K, Kaniwa N (2007) Pharmacogenomics of gemcitabine: Can genetic studies lead to tailor-made therapy? *Br J Cancer* 97:145–151.
22. Sigmond J, Kroep JR, Loves W, Codacci-Pisanelli G, Peters GJ (2004) Quantitative real time PCR of deoxycytidine kinase mRNA by Light Cycler PCR in relation to enzyme activity and gemcitabine sensitivity. *Cancer Lett* 213:173–179.
23. Hubeek I, *et al.* (2005) Immunocytochemical detection of deoxycytidine kinase in haematological malignancies and solid tumours. *J Clin Pathol* 58:695–699.
24. Radu CG, *et al.* (2008) Molecular imaging of lymphoid organs and immune activation by positron emission tomography with a new ^{18}F-labeled 2′-deoxycytidine analog. *Nat Med* 14:783–788.
25. Usova EV, Eriksson S (1997) The effects of high salt concentrations on the regulation of the substrate specificity of human recombinant deoxycytidine kinase. *Eur J Biochemistry/FEBS* 248:762–766.
26. Owens JK, Shewach DS, Ullman B, Mitchell BS (1992) Resistance to 1-β-D-arabinofuranosylcytosine in human T-lymphoblasts mediated by mutations within the deoxycytidine kinase gene. *Cancer Res* 52:2389–2393.
27. Colucci G, *et al.* (2002) Gemcitabine alone or with cisplatin for the treatment of patients with locally advanced and/or metastatic pancreatic carcinoma: A prospective, randomized phase III study of the Gruppo Oncologia dell'Italia Meridionale. *Cancer* 94:902–910.
28. Heinemann V, *et al.* (2006) Randomized phase III trial of gemcitabine plus cisplatin compared with gemcitabine alone in advanced pancreatic cancer. *J Clin Oncol* 24:3946–3952.
29. Pauwels B, *et al.* (2006) The relation between deoxycytidine kinase activity and the radiosensitising effect of gemcitabine in eight different human tumour cell lines. *BMC Cancer* 6:142.
30. Heidel JD, *et al.* (2007) Potent siRNA inhibitors of ribonucleotide reductase subunit RRM2 reduce cell proliferation in vitro and in vivo. *Clin Cancer Res* 13:2207–2215.
31. Heidel JD, *et al.* (2007) Administration in non-human primates of escalating intravenous doses of targeted nanoparticles containing ribonucleotide reductase subunit M2 siRNA. *Proc Natl Acad Sci USA* 104:5715–5721.
32. Duxbury MS, Ito H, Zinner MJ, Ashley SW, Whang EE (2004) RNA interference targeting the M2 subunit of ribonucleotide reductase enhances pancreatic adenocarcinoma chemosensitivity to gemcitabine. *Oncogene* 23:1539–1548.
33. Huang SC, *et al.* (2005) An internet-based ''kinetic imaging system'' (KIS) for microPET. *Mol Imaging Biol* 7:330–341.
34. Adjei AA (2006) Clinical studies of pemetrexed and gemcitabine combinations. *Ann Oncol* 17 (Suppl 5):v29–v32.
35. Dittmann H, *et al.* (2002) Early changes in [^{18}F]FLT uptake after chemotherapy: An experimental study. *Eur J Nucl Med Mol Imaging* 29:1462–1469.
36. Bengala C, *et al.* (2005) Prolonged fixed dose rate infusion of gemcitabine with autologous haemopoietic support in advanced pancreatic adenocarcinoma. *Br J Cancer* 93:35–40.
37. Bergman AM, *et al.* (2005) In vivo induction of resistance to gemcitabine results in increased expression of ribonucleotide reductase subunit M1 as the major determinant. *Cancer Res* 65:9510–9516.
38. Davidson JD, *et al.* (2004) An increase in the expression of ribonucleotide reductase large subunit 1 is associated with gemcitabine resistance in non-small cell lung cancer cell lines. *Cancer Res* 64:3761–3766.
39. Han Z, *et al.* (2008) Noninvasive assessment of cancer response to therapy. *Nat Med* 14:343–349.
40. Rosen MA, Schnall MD (2007) Dynamic contrast-enhanced magnetic resonance imaging for assessing tumor vascularity and vascular effects of targeted therapies in renal cell carcinoma. *Clin Cancer Res* 13:770s–776s.
41. Segal E, *et al.* (2007) Decoding global gene expression programs in liver cancer by noninvasive imaging. *Nat Biotechnol* 25:675–680.
42. Monsieurs M, Brans B, Bacher K, Dierckx R, Thierens H (2002) Patient dosimetry for 131I-MIBG therapy for neuroendocrine tumours based on ^{123}I-MIBG scans. *Eur J Nucl Med Mol Imaging* 29:1581–1587.
43. Hawley RG, Lieu FH, Fong AZ, Hawley TS (1994) Versatile retroviral vectors for potential use in gene therapy. *Gene Ther* 1:136–138.
44. Smal C, *et al.* (2006) Identification of in vivo phosphorylation sites on human deoxycytidine kinase: Role of Ser-74 in the control of enzyme activity. *J Biol Chem* 281:4887–4893.
45. Petty RD, Sutherland LA, Hunter EM, Cree IA (1995) Comparison of MTT and ATP-based assays for the measurement of viable cell number. *J Biolum Chemilum* 10:29–34.
46. Koresawa M, Okabe T (2004) High-throughput screening with quantitation of ATP consumption: A universal nonradioisotope, homogeneous assay for protein kinase. *Assay Drug Dev Technol* 2:153–160.
47. Smal C, *et al.* (2004) New evidences for a regulation of deoxycytidine kinase activity by reversible phosphorylation. *Nucleosides Nucleotides Nucleic Acids* 23:1363–1365.